ISSN 1029-9599, Physical Mesomechanics, 2013, Vol. 16, No. 2, pp. 170–182 © Pleiades Publishing, Ltd., 2013.
Original Russian Text © S.V. Panin, I.V. Vlasov, V.P. Sergeev, A.R. Sungatulin, M.P. Kalashnikov, M.A. Poltaranin, B.B. Ovechkin, 2012, published in Fizicheskaya Mezomekhanika, 2012, Vol. 15, No. 6, pp. 93–106.

Increasing the Fatigue Life of 12Cr1MoV Steel by Surface Nanostructuring with a Zr^+ Ion Beam. Structure, Properties, and Fracture Pattern

S. V. Panin*[1,2], I. V. Vlasov[1,2], V. P. Sergeev[1], A. R. Sungatulin[1], M. P. Kalashnikov[1], M. A. Poltaranin[1,2], and B. B. Ovechkin[2]

[1] *Institute of Strength Physics and Materials Science, Siberian Branch, Russian Academy of Sciences, Tomsk, 634021, Russia*
[2] *National Research Tomsk Polytechnic University, Tomsk, 634050, Russia*
* *svp@ispms.tsc.ru*

Received October 31, 2012

Abstract—The paper presents the results of static and cyclic tensile tests and alternate cyclic bending tests of 12Cr1MoV specimens in the initial state and after surface nanostructuring with a Zr^+ ion beam. Examination by optical and scanning electron microscopy and interference profilometry revealed differences in the formation of the deformation relief and in the character of cracking of the modified surface layer. The changes occurring in the modified surface layer were estimated by nanoindentation, X-ray analysis, and fractography. The nanostructure formed in the treated surface layer was analyzed by transmission electron microscopy. The difference in deformation is interpreted using the multiple cracking concept. The effect of substantial enhancement of fatigue strength is associated with retarded plastic deformation and fatigue crack propagation in the modified surface layer.

DOI: 10.1134/S1029959913020082

Keywords: fatigue, vacuum arc ion beam treatment, nanostructuring, multiple cracking, deformation, fracture.

1. INTRODUCTION

Surface modification is an effective way of both protecting structural materials and enhancing their physicomechanical properties. At the same time, under mechanical loading a difference in the elastic moduli of the modified surface layer and adjacent substrate material causes the appearance of stress concentrators in which stresses relax by localized plastic deformation or by cracking [1]. Under cyclic loading the difference in the properties usually results in the nucleation of (multiple) microcracks in the hardened surface layer, which can be thought of as micronotches [2, 3]. Consequently, the choice of regimes and parameters of surface layer modification depends, as a rule, on its strength/ductility, thickness, and on some other factors.

The ion implantation method has been widely applied in industries for a long time and is now a well studied process [4]. In the last years vacuum arc ion sources are used for surface nanostructuring, which allows the formation of surface layers with a thickness (up to several microns) a few times larger than that formed with the use of conventional ion implantation methods. Such nanostructured surface layers are still coatings in the full sense of the word, but they cannot already be called just an ion implanted layer [5]. Their investigation is of particular interest as they allow a simultaneous improvement of fatigue fracture and wear resistance.

The present paper is aimed at studying the influence of surface nanostructuring of 12Cr1MoV steel with a Zr^+ ion beam on the increase of its fatigue life. The first part of the paper is devoted to the structural aspects of surface layer modification and their influence on fatigue life under cyclic tension and bending of specimens.

2. MATERIAL AND INVESTIGATION PROCEDURE

We studied specimens of heat resistant 12Cr1MoV steel designed for the production of power equipment parts and accessories operating at high temperature (570…585 °C) [6]. This grade of steel was chosen be-

cause it does not undergo structural changes at the temperature at which ion beam nanostructruring of the surface layer is carried out. Besides, the steel is rather ductile, which facilitates the investigation of localized deformation and fracture under cyclic loading due to a more visible manifestation and lower rate of deformation and fracture.

Flat specimens measured $70 \times 10 \times 1$ mm were spark cut from a tube fragment. In the initial state 12Cr1MoV steel has a ferritic-perlitic structure with a characteristic grain size of 30…50 μm (Fig. 1). For fatigue tests use was made of specimens with stress concentrators, i.e. holes of diameter 2 mm at a distance of 50 mm from an edge. In static tests similar specimens as well as dumbbell specimens with the gage part measured $20 \times 5 \times 1$ mm were used.

Specimens for tests were mechanically polished and divided into 2 groups: those in the as-delivered state (henceforward referred to as initial), and those modified with a Zr^+ ion beam. The ion nanostructuring of the surface layer was carried out with a high-current vacuum arc metal ion source on the setup UVN-0.2 Kvant [5]. The specimens were treated within a chamber under a vacuum of no less than 7×10^{-3} Pa with a zirconium ion beam of energy –900 V and ion current density 0.1 mA/cm^2. The time of treatment was 19 min. The substrate holder with the specimens, which was attached to the object stage, was introduced directly into the ion acceleration scheme instead of usual extraction of an isolated ion beam from the implanter. In this case, ions were accelerated in a dynamic self-organizing boundary layer which is an electric double layer formed in the vicinity of the specimen surface at negative potential.

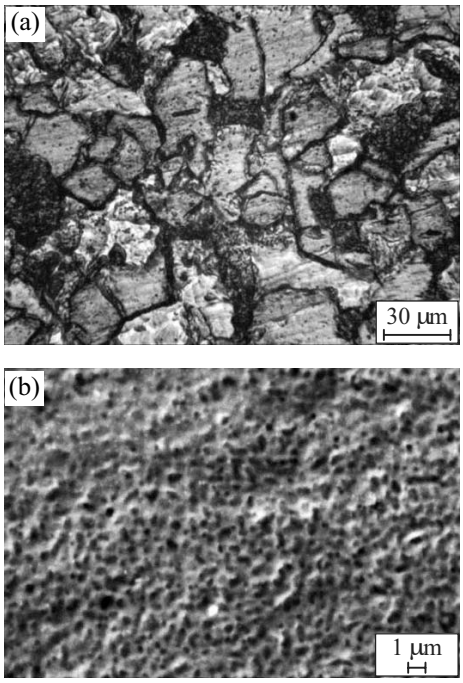

Fig. 1. Optical image of the specimen surface in the as-delivered state after etching (a); SEM image of the specimen surface after Zr^+ ion beam treatment (b).

The specimen microstructure was investigated by chemical etching in a 5% nitric acid solution. The specimen surface images were obtained with the use of an optical microscope Carl Zeiss Axiovert 25 CA, microscope Carl Zeiss EPIQUANT, and scanning electron microscope Carl Zeiss EVO 50. Surface profilometry was performed with a white light interferometer NewView 6200. X-ray analysis was performed with a general-purpose X-ray diffractometer DRON-7.

Static tensile tests were carried out on an electromechanical machine Instron 5582, and cyclic tensile tests—on a servohydraulic testing machine Biss UTM 150. In the fatigue tests, surfaces were photographed with a digital camera Canon EOS 550D to evaluate deformation by an optical method and to describe the surface deformation relief. The specimen nanohardness was measured with the Nanotest system (Micromaterials Ltd.). Two schemes of fatigue testing were applied:

1. Cyclic tension: in the high cycle fatigue regime the maximum load was 2.5 kN and the minimum—0.9 kN; in the low cycle fatigue regime the maximum load was 2.7 kN and the minimum—0.9 kN.

2. Alternate cyclic (cantilever) bending (oscillation amplitude—6 mm, beam length—51 mm, frequency—9.5 Hz).

3. EXPERIMENTAL RESULTS

3.1. Investigation of the modified surface

3.1.1. Electron microscopic investigation

Figure 1b shows the electron microscopic image of the specimen surface nanostructured with a Zr^+ ion beam. It is seen that after such treatment the surface layer structure becomes heterogeneous, with the formation of fine size particles, most probably submicron size zirconates.

Then, the specimens were examined with light transmission microscopy. The surface layer structure of steel in the initial state consists of coarse ferrite grains >1 μm in size with cementite (Fe_3C) inclusions of an average size of 120 nm (Fig. 2a). The structure of steel after nanostructuring with a Zr^+ ion beam consists of $FeZr_2$ and Fe_3Zr phases as well as of ferrite grains. The average size of the Zr-based phases in the surface layer is ~100 nm

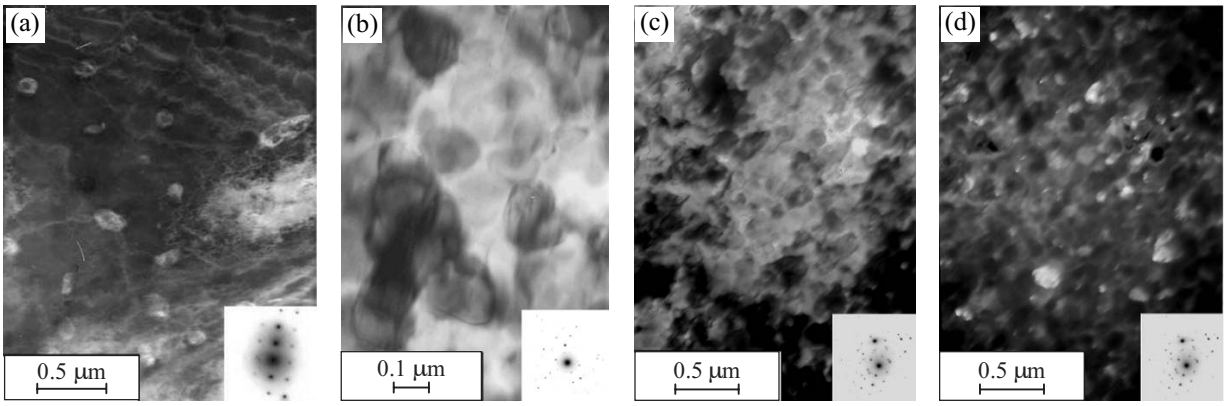

Fig. 2. Electron microscopic image of the subsurface layer structure of 12Cr1MoV steel in the as-delivered state (a) and after nanostructuring (b–d): light (b, c) and dark field (a, d).

(Figs. 2b–2d), though the number of finer size particles is large.

3.1.2. Nanoindentation of specimens

Specimen hardness was measured prior to and after treatment by nanoindentation to a depth of no more than 200 nm. Analysis of the load dependence of the indentation depth for both types of specimens showed that specimen hardness in the initial state comprises ~4.9 GPa. After nanostructuring two types of measurement data can be differentiated for the subsurface layer: average hardness ~5 GPa (which, in our opinion, corresponds to the matrix material), and ~10…12 GPa, which is most probably due to the fact that the indenter pyramid "hits" reinforcing particles. On average (integrally), the subsurface layer hardness increased ~1.4 times.

3.1.3. X-ray investigation

Treated and untreated specimens were X-ray investigated. Figure 3 shows the X-ray diagram for a specimen with the modified surface layer. Before treatment the specimen structure is mainly α-iron, while after nanostructuring metastable intermetallic phases in the Fe–Zr system ($FeZr_2$ and $FeZr_3$) as well as zirconium carbides (ZrC) are found in the subsurface layer. The surface of the specimen with the nanostructured surface layer was subjected to structural phase microanalysis, the results are given in Table 1. The data show that the total zirconium content in the subsurface layer of the treated specimen is about 14.2%.

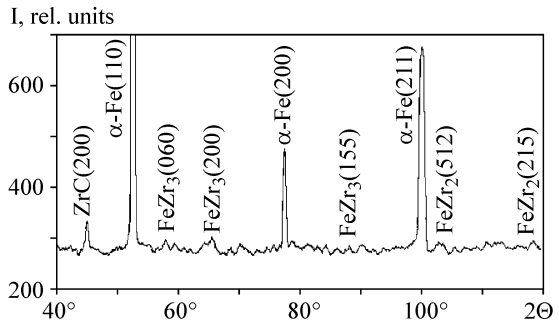

Fig. 3. X-ray diagram of a specimen after treatment.

3.2. Static tensile tests

3.2.1. Mechanical properties

Figure 4a illustrates the tensile stress-strain diagram for 12Cr1MoV steel dumbbell specimens. It is seen that for the untreated specimens the curve has a yield plateau typical of low-carbon steel deformation. The yield strength for such specimens is $\sigma_{0.2} = 387 \pm 23$ MPa, the ultimate strength $\sigma_в = 494 \pm 36$ MPa, and the tensile strain $\varepsilon = 22 \pm 3$ %; these values are close to the tabular data for the given steel [6]. After surface layer modification the ultimate strength reaches $\sigma_в = 570 \pm 17$ MPa and the tensile strain $\varepsilon = 16 \pm 0.7$%, with no yield plateau for the treated specimens (Fig. 4*a*). So, nanostructuring leads to ultimate strength increase by ~75 MPa (15%) and tensile strain decrease by $\varepsilon = 4$% (19%).

Tensile tests were performed on specimens with a hole as a stress concentrator (Fig. 4*b*). The average ultimate strength for the specimens in the as-delivered state is seen to be $\sigma_в = 490 \pm 25$ MPa. For the treated speci-

Table 1. X-ray microspectral analysis data for the surface layer nanostructured with a Zr^+ ion beam

Element	Cr	Fe	Zr
Average content, %	1.25	84.55	14.21

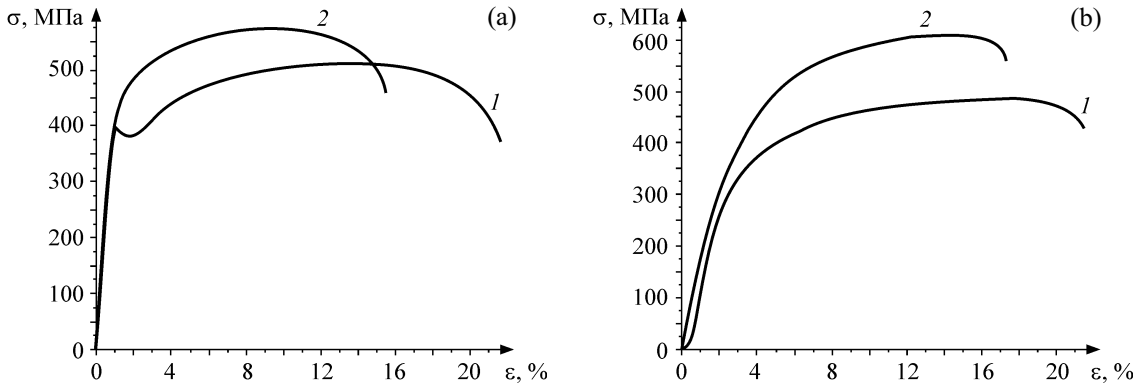

Fig. 4. Stress-strain diagram in tension of 12Cr1MoV steel specimens in the form of a dumbbell (a) and a plate with a hole (b): *1*—specimen in the as-delivered state, *2*—with nanostructured surface layer.

mens $\sigma_в = 615 \pm 40$ MPa. The ultimate strength and tensile strain values for the specimens in the as-delivered state with a hole and without it differ insignificantly. For the nanostructured specimen with a stress concentrator the ultimate strength increased by 125 MPa (20%), and the tensile strain decreased by 4% (19%). The tensile stress-strain diagrams for the specimens with a hole has no yield plateau both in the as-delivered and modified state (Fig. 4b). So, independently of specimen shape and changing stress-strain state distribution in the presence of a hole, specimen strength increases after surface layer nanostructuring, while ductility decreases.

3.2.2. Optical microscopy

Fracture surface images of dumbbell specimens subjected to static tension were analyzed (Figs. 5a and 5c). For the untreated specimens the reduction of the gauge cross-section area is $\psi = 29\%$, while after nanostructu-

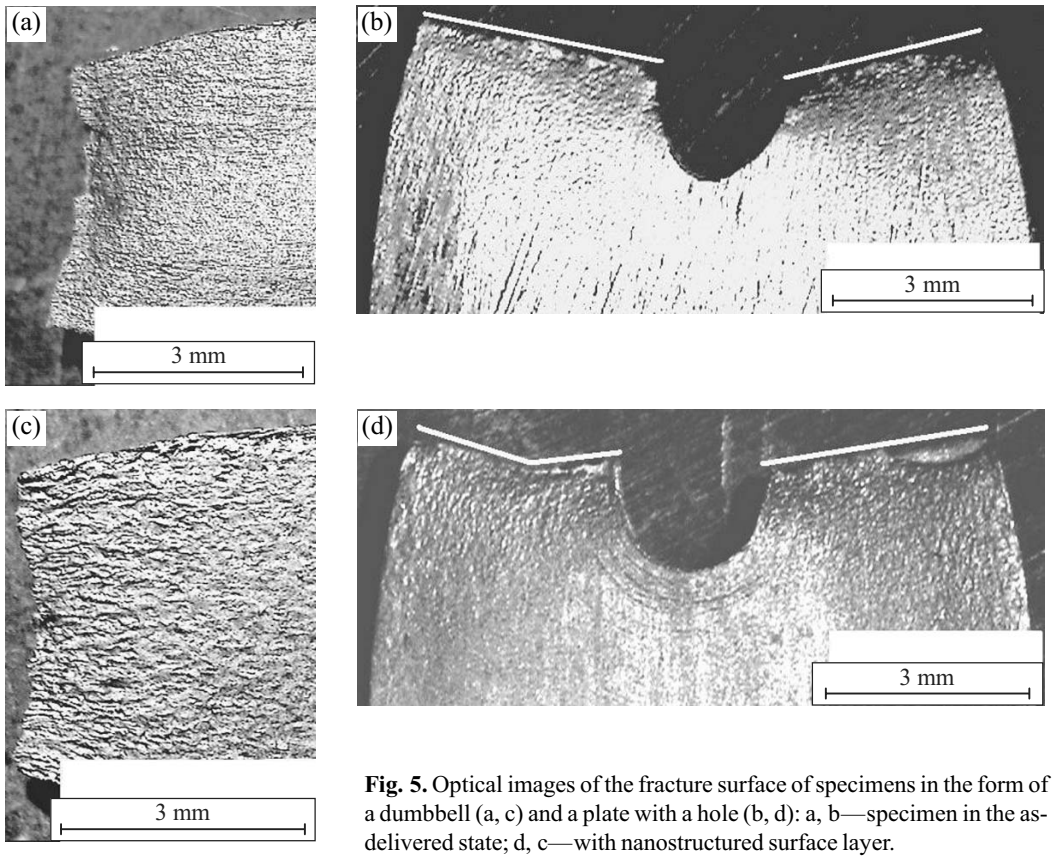

Fig. 5. Optical images of the fracture surface of specimens in the form of a dumbbell (a, c) and a plate with a hole (b, d): a, b—specimen in the as-delivered state; d, c—with nanostructured surface layer.

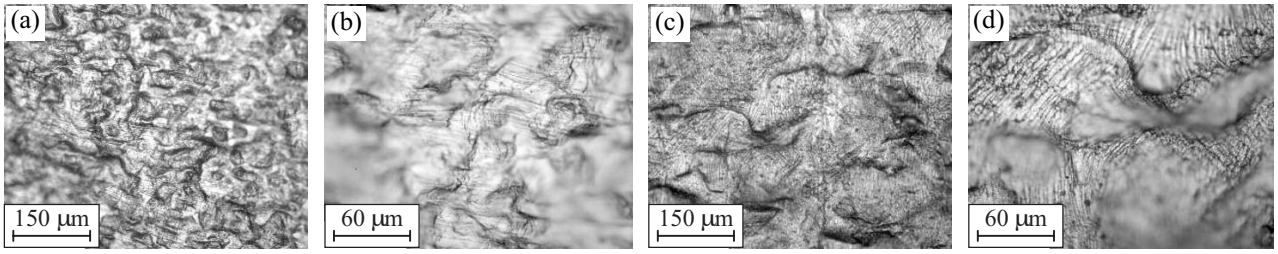

Fig. 6. Optical images of the fracture surface of specimens tested under static tension: untreated specimens (a, b) and subjected to surface nanostructuring (c, d); tension axis is oriented horizontally.

ring this parameter reduced to $\psi = 26\%$. In the untreated specimen, the deformation relief is rather uniformly distributed over the gauge section and has finer elements (Fig. 5a); in the specimen with the nanostructured surface layer, the deformation relief in the neck region is more well-defined and exhibits coarser elements (Figs. 5c and 5d).

Figures 5b and 5d demonstrate the fracture surface of specimens with a hole as a stress concentrator. The white lines indicate the fracture plane. The degree of plastic deformation of the untreated specimen is seen to be much higher, which is manifested in its greater elongation. The cross-section area reduction in the untreated specimen was $\psi = 15.5\%$, while in the specimen with the modified surface layer $\psi = 13.9\%$. Another essential difference in the deformation and fracture patterns is that in the untreated specimen the main crack propagates uniformly over the cross-section, while in the specimen with the modified surface layer the crack initially propagates like a fatigue crack (along the normal to the tension axis and then in the tension direction, Fig. 5d).

The specimen surface near the region of the main crack propagation at a distance from the fracture edge was examined microscopically (Fig. 6). The untreated specimen surface has a well-defined grain-like relief (Figs. 6a and 6b). The specimens with the nanostructured surface layer have randomly oriented fine cracks in the modified layer (Figs. 6c and 6d). The presence of the modified layer on the surface of steel 12Cr1MoV hinders the formation of an original grain-like relief on the substrate, which reduces the surface roughness of such specimens (see optical profilometry data below).

3.2.3. Electron microscopic study of the fracture surface

The surface of the specimens subjected to static tension was examined with a scanning electron microscope (Figs. 7a, 7b, 7d, and 7e). Since under static tension the specimen gauge section undergoes significant plastic elongation due to localized deformation, the electron microscopic examination was performed mainly in this part of the specimen which exhibited severe plastic deformation.

It is seen that fracture of the modified layer (whose thickness can be estimated in units of micrometers) is brittle and accompanied by multiple microcracking of the nanostructured layer. Particular attention must be paid to the lower part of the micrograph given in Fig. 7e. Beneath the cracked hardened layer whose small fragments are detached from the substrate there are lamellae of the extruded substrate material not oriented normally to the tensile direction. A similar result was earlier described in paper [7] for the case of tensile low-carbon steel specimens with a subsurface layer nanostructured by ultrasonic treatment. It was shown in the paper that the generation of a special nanostructural state during deformation leads to the formation of peculiar strain-induced mesoscopic defects, namely, double spirals of extruded material. When thin coatings or modified layers are formed on the surface, the propagation of such strain-induced mesoscopic defects is manifested as plastic shear channeling [8] and causes multiple cracking, with (micro)cracks oriented in directions different from the loading direction. As a result, both the strength and ductility of specimens may increase simultaneously.

The fracture surface shows the signs of ductile fracture, except for the surface layer whose fracture was more brittle (Fig. 8f). Obviously, the thickness of the given layer is not a strictly constant value; it is manifested in a varying thickness of the subsurface layer characterized by brittle fracture (the layer resembles the "crust" of solid material near the specimen surface). According to contemporary notions of the physical mesomechanics of materials such a discontinuity can be interpreted as structural-phase decomposition in the conditions of brittle-ductile fracture [10].

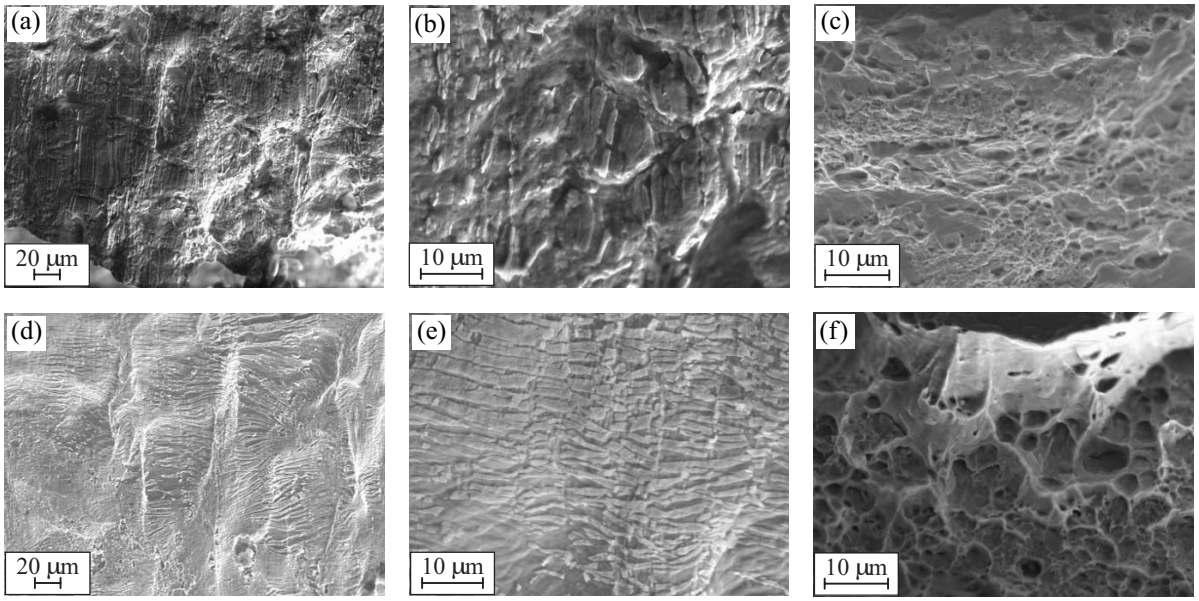

Fig. 7. SEM micrographs of the hardened surface (a, b, d, e) and fracture surface (c, f) of specimens tested under static tension: untreated specimen (a–c) and specimen with nanostructured surface layer (d–f); a, b, d, e—tension axis is oriented vertically.

3.3. Cyclic tensile tests

3.3.1. Low cycle fatigue regime

The results of cyclic tensile tests have shown that in the low cycle fatigue regime the number of cycles to failure for specimens with the modified surface layer increased ~3 times: from 42×10^3 to ~150×10^3 cycles (Fig. 8b). Simultaneously, the time to crack nucleation also increased ~3 times. As one can see from the diagram plotted for the normalized number of loading cycles, there are no great differences in the pattern of crack growth for untreated specimens and those with the modified surface layer (Fig. 8a). The major differences occur in the period of time preceding the main crack nucleation (Fig. 8b). In a specimen with the nanostructured surface layer the crack nucleates much later and propagates more slowly.

By the plotted diagrams we calculated the crack growth rate in the specimens. The crack growth rate for an untreated specimen is 0.26 μm/cycle, and after surface layer nanostructuring it attains 0.052 μm/cycle. The modified layer effectively inhibits fatigue crack nucleation and increases 3 times the number of cycles to crack nucleation; it also inhibits the crack growth making it 5.5 times slower and thus reducing the size of the plastic elongation region.

To study in more detail the processes that accompany the nucleation and propagation of fatigue cracks, we ex-

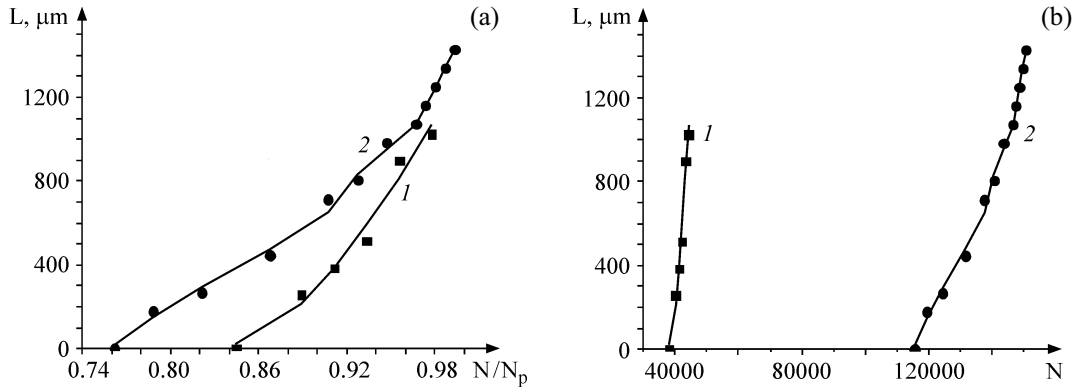

Fig. 8. Dependence of the crack length on the normalized (a) and absolute number of cycles (b): *1*—untreated, *2*—with nanostructured surface layer.

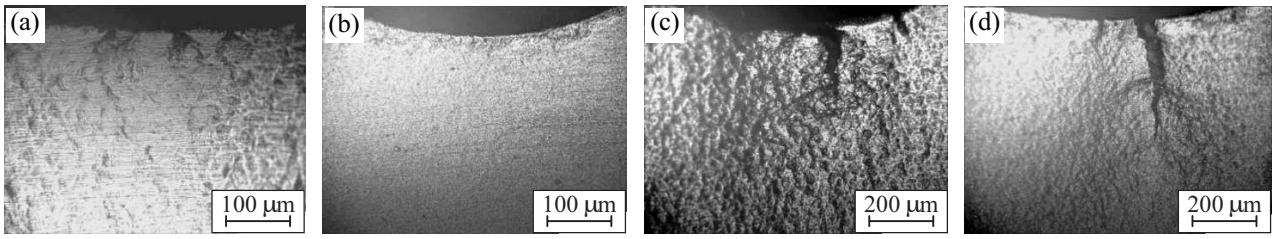

Fig. 9. Optical surface images of the untreated specimen (a, c) and with nanostructured surface layer (the hole is at the top) (b, d) after $N = 3 \times 10^3$ (a, b), 27×10^3 (c), 48×10^3 cycles (d).

amined them closely with an optical microscope; to do this, we removed specimens from the testing machine clamps during mechanical loading and photographed them. It is seen (Fig. 9a) that after $N = 3\,000$ cycles a well-defined deformation relief appears on the untreated specimen surface, which mostly inherits the grain-like pattern. Besides, the stress concentrator region brought into sharp focus demonstrates crack nucleation and local variation of specimen thickness (Fig. 9c), which is related to severe plastic deformation in this region. For the specimen with the modified surface layer, no considerable changes are observed at the same number of cycles (Fig. 9b). Under further loading the formation of the deformation relief on the untreated specimen surface continues. The stress concentrator region is characterized by a coarse stepped relief showing up as the height difference induced by local thinning of the specimen and fatigue crack initiation (Fig. 9c). The nanostructured specimen surface has a less well-defined deformation relief. The propagation of the main fatigue crack begins shortly before fracture (Figs. 9d and 8b).

Using the optical microscopy data we measured the relative plastic elongation of the gauge section for both types of specimens: in the untreated specimen it was $\psi = 18\%$, and after nanostructuring $\psi = 13\%$ (Figs. 10a and 10d). Recall that for the case of static tension the difference in the relative elongation was much less: $\psi = 15.5\%$ versus $\psi = 13.9\%$. The plastic elongation of the untreated specimen is seen to be higher after fatigue testing (Figs. 10a and 10d). The relative elongation values for the treated specimens did not change significantly. This can be due to the fact that the nanostructured surface layer inhibits homogeneous plastic deformation. It is also seen that under cyclic loading the relative elongation of the specimen with the modified surface layer is lower compared to the untreated specimen, and the size of the region involved in severe plastic deformation is smaller (the zone of elongation and ultimate fracture (Figs. 10a and 10d).

In general, the way of how the plastic elongation region is formed resembles that under static tension, being of no special interest to us. Hence further we consider the zone of fatigue crack growth where the process of the formation of deformation relief differs strongly for untreated specimens and those with the nanostructured surface layer. The crack growth zone was analyzed metallographically at higher magnification. Figures 10*b*, 10c, 10e, and 10f illustrates the fracture surface of an untreated specimen and specimen with the nanostructured surface layer. The fracture of the untreated specimen shows the signs of plastic deformation around the fatigue crack; the deformation relief is coarse and well-defined (Fig. 10b). At the same magnification the treated specimen has no visible signs of plastic deformation, and fatigue fracture occurs in a more brittle way (Fig. 10e). To obtain higher contrast images, the surface was photographed using dark field illumination at a short distance from the stress concentrator (Figs. 10c and 10f). The deformation relief of the treated specimen is fine and more homogeneous than that of the untreated specimen where folds and cracks are much larger in size.

3.3.2. High cycle fatigue regime

The results of cyclic tensile tests in the high cycle fatigue regime have shown that the number of cycles to failure for specimens with the nanostructured surface layer increased twice compared to the untreated ones (Fig. 11), and simultaneously the time to crack nucleation increased ~2 times. Using the obtained optical images, we calculated and plotted the dependence of the crack length on the normalized (Fig. 11a) and absolute number of tension cycles (Fig. 11b). Like in the low cycle fatigue regime, the normalized coordinates do not differ significantly; the main differences are in the time of fatigue microcrack nucleation and in the rate of the main crack propagation. According to rough estimates made on the basis of a linear approximation of the curves given in Fig. 11b, the crack propagation rate in untreated specimens

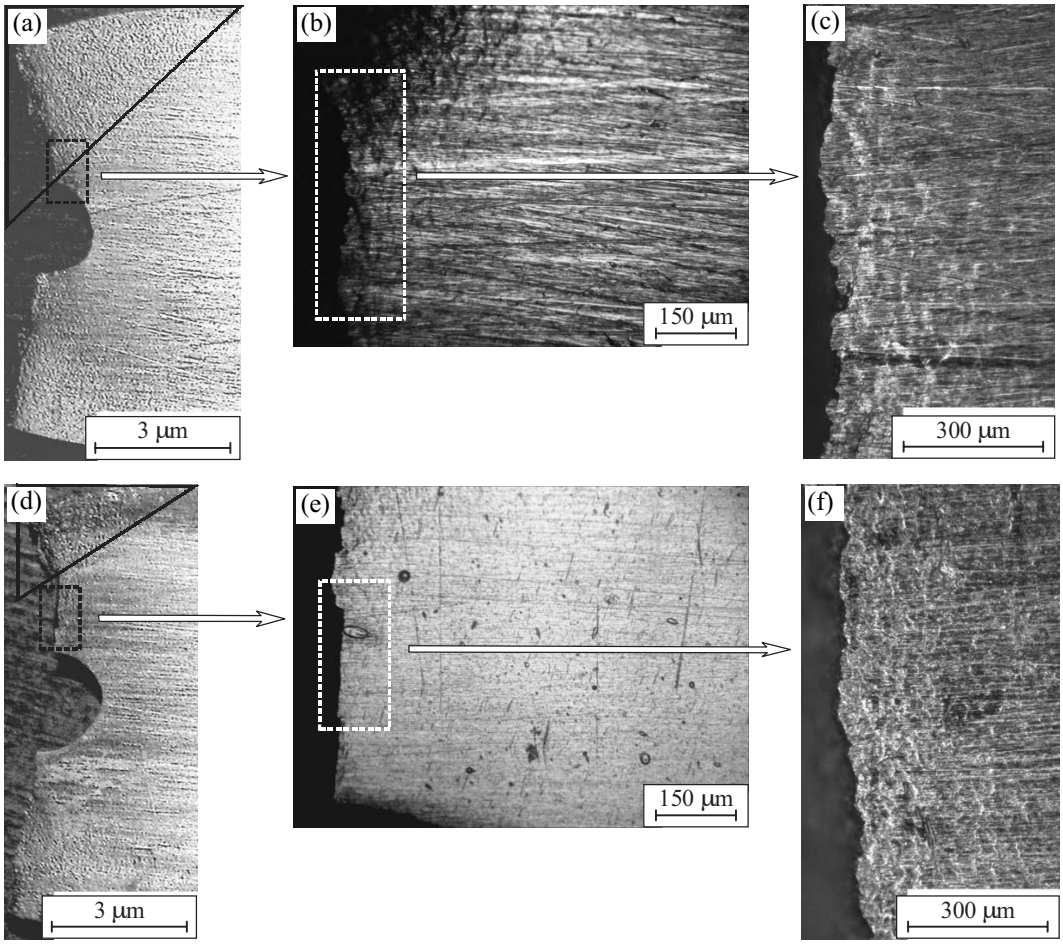

Fig. 10. Optical surface images of cyclically tested untreated (a–c) and ion-beam nanostructured (d–f) specimens.

was 0.1 μm/cycle, while after surface layer nanostructuring it reduced almost twice down to ~0.05 μm/cycle.

The optical microscopy data were used to analyze the deformation relief. The untreated specimen fracture occurs with the signs of plastic deformation around the fatigue crack, and the deformation relief is coarse and well-defined (Fig. 12a). At the same magnification the treated specimen shows no signs of plastic deformation, and the character of fatigue crack growth is more brittle (Fig. 12b). At higher magnification the nanostructured

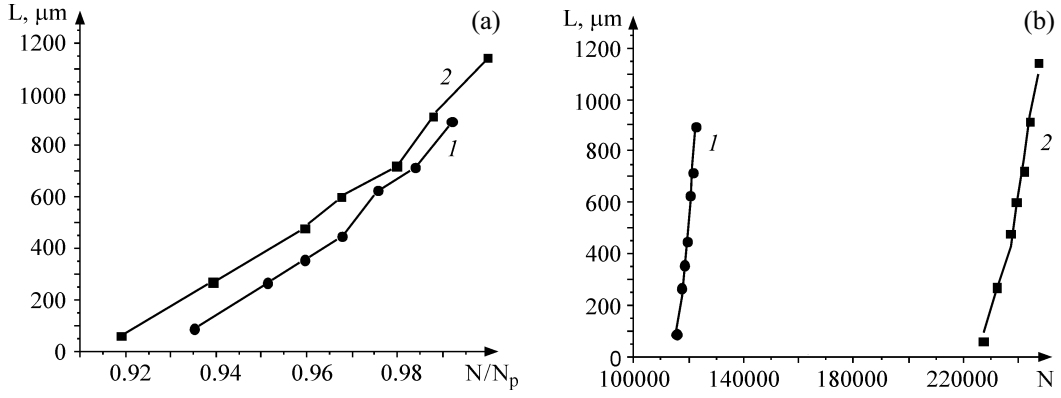

Fig. 11. Dependence of the crack length on the normalized (a) and absolute number of cycles (b) in the as-delivered state (*1*) and with nanostructured surface layer (*2*).

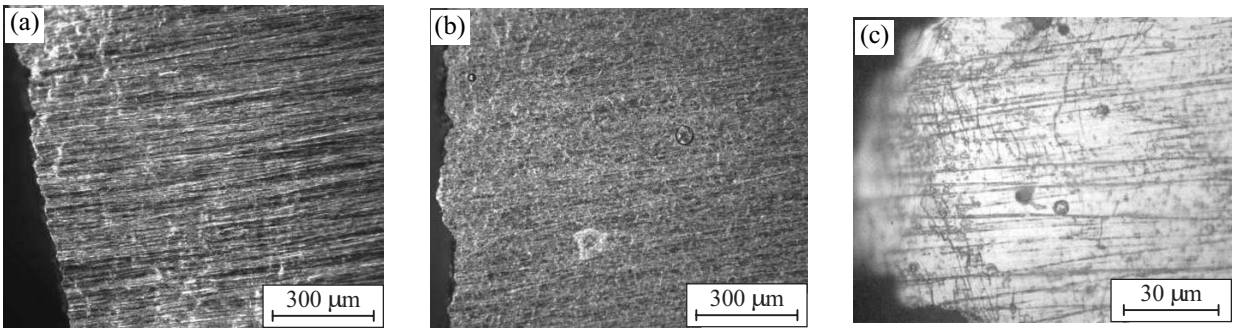

Fig. 12. Optical surface images of cyclically tested untreated (a) and ion-beam nanostructured (b, c) specimens.

layer exhibits multiple cracks in the fatigue crack growth region at the fracture edge of the specimen (Fig. 12c). Specimens with the nanostructured surface layer also have a system of fine microcracks which evidently appear in the zones related to the boundaries of individual grains in the underlying substrate layer, while the deformation relief is much less defined. The sharp-focused image of the untreated specimen shows slip traces in the vicinity of individual grains. Notice that the specimen with the modified surface layer must be considered at least as a two-level system, in which deformation in each of the conjugated layers is governed by its internal structure, and the need for consistent deformation in the ductile substrate gives rise to specific deformation processes in the harder modified surface layer.

The specimens failed in cyclic tensile tests were examined and photographed on a scanning electron microscope at high magnification (Fig. 13). The micrographs of the fatigue crack growth region (Fig. 13d) also testify that fracture of the nanostructured surface layer is brittle in contrast to the untreated specimen (Fig. 13a). It is seen (Fig. 13e) that fine cracks are formed in the nanostructured layer, which is not accompanied by noticeable localization of deformation. According to paper [10], multiple cracking assists in load redistribution and minimizes the influence of the strong stress macroconcentrator acting in the zone of the main fatigue crack propagation. It should be inferred that the modified surface layer impedes the formation of zones of local curvature and, consequently, retards for a long time the structural-

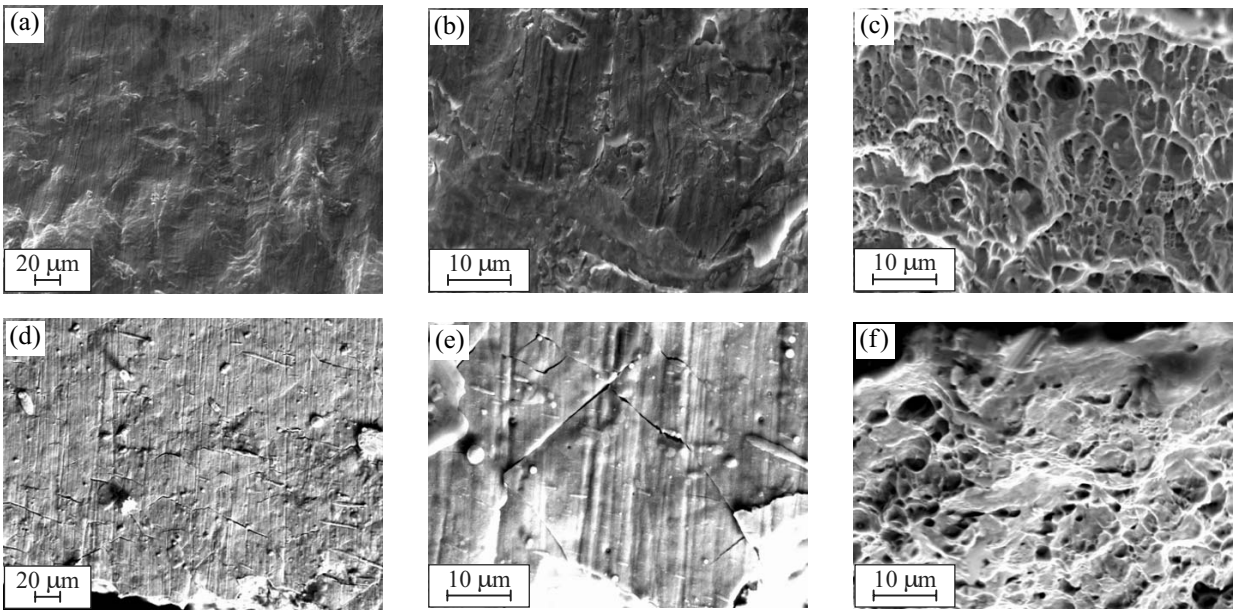

Fig. 13. SEM micrographs in the zone of fatigue crack growth on the plane face (a, b, d, e) and fracture surface (c, f) of specimens tested under cyclic tension: a–c—untreated specimen; d–f—specimen with nanostructured surface layer.

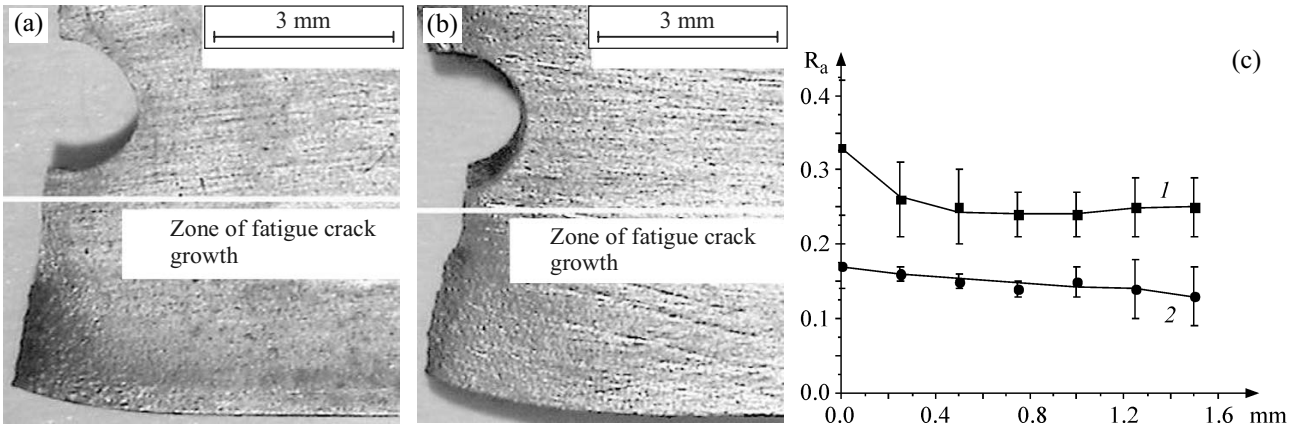

Fig. 14. Optical images of the untreated specimen surface (a) and modified specimen surface (b) (high cycle fatigue regime), and dependence of roughness parameter R_a on the distance from the fracture surface along the cross section designated by the white line in Figs. 14a and 14b (c): untreated specimen (*1*) and specimen with nanostructured surface layer (*2*).

phase decomposition of the substrate material, thus slowing down the nucleation of fatigue (micro)cracks.

Figures 13c and 13f shows the fracture surfaces of untreated specimens ($N_p = 119.5 \times 10^3$) cycles to failure in the high cycle fatigue regime) and specimens with the nanostructured surface layer ($N_p = 151.5 \times 10^3$) cycles to failure in the low cycle fatigue regime). The micrographs of the untreated specimen demonstrate that fracture all over the observed area is ductile. Noticeable is the low porosity typical for the fracture surface of such a specimen (Fig. 13c). As for the specimen with the nanostructured surface layer (Fig. 13f), its fracture is quasibrittle (which can be interpreted as the propagation of an opening mode crack in the three-dimensional stress state [9]). At higher magnification the fracture surface of this specimen clearly demonstrates a quasi-brittle type of fracture.

The surface of specimens with a hole failed in cyclic tension was examined with an optical profilometer. We analyzed the fatigue crack growth region in the immediate vicinity of the stress concentrator represented by the hole (Fig. 14a). The white line in Figs. 14b and 14c indicates the cross section where the roughness parameter R_a was measured (Fig. 14c). Plastic deformation (and, consequently, roughness) in this region on the specimen surface is seen to be minimum. The values of the roughness parameter R_a for a specimen with the nanostructured surface layer are lower. This difference is especially evident near the fracture edge (Fig. 14c).

3.4. Alternate cyclic bending tests

According to the obtained test results, the fatigue life of specimens under alternate cyclic bending increased

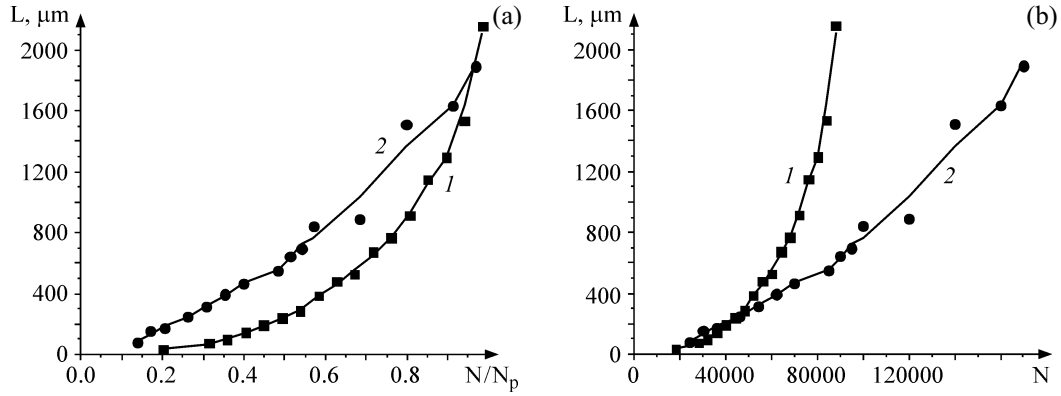

Fig. 15. Dependence of the crack length on the normalized (a) and absolute number of cycles (b): *1*—untreated specimen; *2*—with nanostructured surface layer.

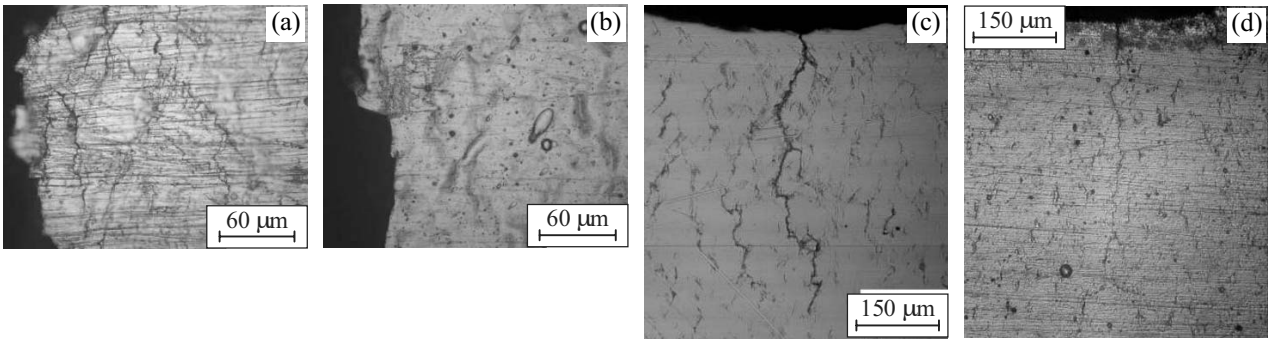

Fig. 16. Optical surface images that illustrate evolution of the deformation relief (a, b) and crack propagation (c, d): a, c—untreated specimen; b, d—with nanostructured surface layer.

2 times due to surface layer nanostructuring. By the obtained optical images, we plotted the dependences of the crack length on the normalized and absolute number of bending cycles (Fig. 15). The diagram for the normalized number of loading cycles shows that there are no significant differences in the character of crack growth for both types of specimens (Fig. 15a). The main differences become evident when the main crack starts to propagate (Fig. 15b), in the diagram for the absolute number of cycles. The calculated crack growth rate is 0.053 μm/cycle for an untreated specimen and 0.014 μm/cycle for a specimen with the nanostructured surface layer. As one can see, the modified layer reduces ~3 times the crack propagation rate.

The deformation relief was studied optically. Figure 16 demonstrates both types of specimen surface made at different number of cycles to failure. The deformation relief of the specimens subjected to alternate cyclic bending was analyzed (Figs. 16a and 16b). It is seen that in the untreated specimen extended thin folds are formed near the zone of fracture (Fig. 16a) which promote (micro)cracking. The number of such folds in the nanostructured layer is much less, and the deformation relief is smoother and varies more continuously (Fig. 16b). The images in Figs. 16c and 16d illustrate the fatigue crack propagation in both types of specimens. The specimens were subjected to different loads: the untreated specimen was loaded for 58×10^3 cycles (Fig. 16c), and that with the nanostructured surface—for 95×10^3 cycles (Fig. 16d). In the images the crack length is roughly similar to illustrate differences in both types of specimens. In the untreated specimen apparent cracks are formed at grain boundaries, and the main crack is more well-defined and probably opens larger. In the treated specimen there are almost no microcracks (except for the main crack), and the relief looks smoother. The more well-defined main crack in the untreated specimen indicates that the crack propagates both on the surface and in the bulk of the material. The main crack in the nanostructured specimen is less well-defined. This may also corroborate the fact that the modified layer impedes its propagation.

The surface roughness near the zone of fracture was measured in the specimens upon failure. The surface roughness parameter ($R_a = 0.490$ μm) for the untreated specimen turned to be more than 1.5 times higher ($R_a = 0.710$ μm) than that for the specimen with the nanostructured surface layer.

4. DISCUSSION OF RESULTS

The paper reveals that under cyclic tension the presence of a nanostructured surface layer strongly impedes the formation of the deformation relief on the surface of 12Cr1MoV steel specimens, and hence the time to fatigue crack nucleation can be reduced more than twice. In our opinion, this is an explanation of fatigue strength enhancement in such specimens. In the case of cyclic bending the time to fatigue crack nucleation in both types of specimens is nearly the same. However, the presence of a nanostructured surface layer, when it is alternately subjected to tensile and compressive stresses, impedes crack propagation in a specimen; as a result, the number of cycles to fatigue failure in such specimens also increases twice in comparison with that for the untreated specimens. The given effect is probably due to the fact that such a layer, on the one hand, is harder owing to the formation of a large number of fine particles of the reinforcing phase (which is confirmed by nanohardness measurement data and by a retarded formation of the deformation relief under loading). On the other hand, these particles are embedded in a ductile metal matrix, which

makes the layer less brittle, and in combination with small thickness its fracture is not accompanied by failure or looks like multiple microcracking (at high degrees of strain) that eliminates macrolocalization of deformation.

Fatigue fracture occurs under elastic loading of a specimen, however, thin surface layers experience plastic deformation in the field of maximum tangential stresses. Their incompatibility causes the formation of fatigue cracks in surface layers [11–16, et al.]. Since a crack is the rotational mode of deformation at the macroscale level, it may nucleate and grow only when rotational modes of deformation occur at mesoscale levels. Such conditions are analyzed on the basis of the relationship [13]

$$\sum_{i=1}^{N} \mathrm{rot}\, I_i = 0, \qquad (1)$$

where I_i are the defect fluxes that govern the rotational modes of deformation at the *i*-th structural scale level.

It is common knowledge that surface layer nanostructuring of structural materials or deposition of nanostructured coatings increase the fatigue life of the materials [5]. However, each particular case requires special analysis of the enhancement mechanisms on the basis of relationship (1). Let us consider our investigation results from this point of view.

The formation of stable carbide ZrC and metastable phases $FeZr_2$, $FeZr_3$ in the surface layer increases 1.5 times the coating hardness and determines its brittleness. This hinders plastic flow development in the surface layer. Along with this, the nanostructure of the coating and its multiple cracking are a damping factor that prevents the nucleation and propagation of the main fatigue crack at the coating–steel substrate interface. All the above factors increase 2–3 times the fatigue life of steel with the Zr-implanted surface layer.

Differences in the character of fatigue crack nucleation and growth under cyclic tension and cyclic bending become clear as well. In the first case, the major role belongs to the delayed nucleation of the fatigue crack because the brittle coating is not subjected to bending stresses but effectively inhibits plastic flow of the surface layer. In the second case, the maximum tensile load at specimen bending leads to a rapid nucleation of the fatigue crack in the brittle coating. Under alternate bending the crack may propagate along a zigzag trajectory only [12]. The conjugation of a ductile heat-resistant steel substrate and high-strength coating impedes the zigzag crack propagation, which also contributes to a 2–3-fold increase of fatigue strength of the steel specimen with the hardened surface layer.

A very important information about the influence of the hardened nanostructured surface layer on the fracture mechanics of the specimen is provided by fractography of fracture surfaces (Figs. 13c and 13f). The uncoated specimen demonstrates ductile fracture (Fig. 13c), when the fatigue crack propagates in the conditions of severe plastic deformation at the crack tip, which causes high vorticity of the deformed material. The fatigue failure of the specimen with the modified surface layer is related to the propagation of an opening mode crack under plane strain in the conditions of three-dimensional stress state. The deformation relief of flat specimen surfaces (Fig. 13) clearly demonstrates differences in the stress-strain state of the coated and uncoated specimen at fatigue failure.

5. CONCLUSION

Zirconium ion beam nanostructuring of the surface layer of 12Cr1MoV steel specimens enhances ultimate strength by 15% and reduces elongation to failure by ~6%. For the treated specimens, the number of cycles to fatigue failure under cyclic tension increases 2–3 times. The cause of the increase is, first of all, related to a delayed nucleation of the main crack. After the crack nucleation, failure of the untreated specimens and specimens with the nanostructured surface layer occurs in a similar way.

Under cyclic tension the untreated specimen demonstrates a coarse deformation relief. It is such relief that determines earlier initiation of (micro)cracks and reduces fatigue strength. Fracture of the nanostructured surface layer is not accompanied by strain macrolocalization and is characterized by multiple fine cracking.

Under alternate cyclic bending the untreated specimen demonstrates a well-defined coarse deformation relief in the form of folds and cracks. In the nanostructured specimen the surface deformation relief is less well-defined, the surface roughness is 1.5 times lower than that of the untreated specimen, and surface deformation is more uniform. The presence of the nanostructured surface layer impedes the growth of the surface fatigue crack under cyclic bending, which is the cause of fatigue strength increase in such specimens.

The work has been financially supported by the RAS Department of Energy, Engineering, Mechanics and Control Processes (Project No. 12.3), SB RAS Projects III.23.1.3 and III.23.1.1, and Project of the Ministry of Education and Science of the Russian Federation, government contract No. 16.552.11.7063.

REFERENCES

1. Panin, V.E., Physical Mesomechanics of Solid Surface Layers, *Phys. Mesomech.*, 1999, vol. 2, no. 6, pp. 5–21.
2. Tushinskii, L.I., Plokhov, A.V., Stolbov, A.A., and Sindeev, V.I., *Structural Strength of the Substrate–Coating Composition*, Nauka: Novosibirsk, 1996.
3. Bydzan, A.Yu., Panin, S.V., and Durakov, V.G., A Study of the Fatigue Failure Mechanisms of 20Cr13 Structural Steel and Its Compositions with Surfaced Coatings, *Phys. Mesomech.*, 2003, vol. 6, no. 1–2, pp. 41–52.
4. Didenko, A.N., Sharkeev, Yu.P., Kozlov, E.V., and Ryabchikov, A.I., *Effects of Long-Range Action in Ion-Implanted Metallic Materials*, Tomsk: Izd-vo NTL, 2004.
5. Panin, V.E., Sergeev, V.P., and Panin, A.V., *Surface Layer Nanostructuring of Structural Materials and Nanostructured Coating Deposition*, Tomsk: Izd-vo TPU, 2008.
6. Zubchenko, A.S., Koloskov, M.M., Kashirskii, Yu.V., et al., *Grade Guide for Steels and Alloys*, Zubchenko, A.S., Ed., Moscow: Mashinostroenie, 2003.
7. Panin, V.E. and Panin, A.V., Effect of the Surface Layer in a Solid under Deformation, *Phys. Mesomech.*, 2005, vol. 8, no. 5–6, pp. 7–14.
8. Panin, V.E., Egorushkin, V.E., and Panin, A.V., The Plastic Shear Channeling Effect and the Nonlinear Waves of Localized Plastic Deformation and Fracture, *Phys. Mesomech.*, 2010, vol. 13, no. 5–6, pp. 215–232.
9. Panin, V.E., Egorushkin, V.E., Derevyagina, L.S., and Deryugin, E.E., Nonlinear Wave Processes Involved in Crack Propagation in Brittle and Brittle-Ductile Fracture, *Fiz. Mezomekh.*, 2012, vol. 15, no. 6, pp. 5–13.
10. Panin, V.E., Goldstein, R.V., and Panin, S.V. Mesomechanics of Multiple Cracking of Brittle Coatings in a Loaded Solid, *Int. J. Fract.*, 2008, vol. 150, pp. 37–53.
11. Terent'ev, V.F., *Fatigue of Metallic Materials*, Moscow: Nauka, 2003.
12. Panin, V.E., Elsukova, T.F., and Popkova, Yu.F., Physical Fundamentals of Mesomechanics of a Two-Layer Composite: Development of Fatigue Cracking, *Dokl. Phys.*, 2012, vol. 57, no. 3, pp. 100–103.
13. Panin, V.E., The Physical Foundations of the Mesomechanics of a Medium with Structure, *Russ. Phys. J.*, 1992, vol. 35, no. 4, pp. 305–315.
14. Panin, V.E., Elsukova, T.F., Egorushkin, V.E., et al., Deformation Mechanisms and Mass Transfer in Highly Non-Equilibrium Polycrystals under Alternate Bending, *Deformats. Razrush.*, 2009, no. 6, pp. 2–12.
15. Shanyavskii, A.A., *Modeling of Metal Fatigue Fracture. Synergetics in Aviation*, Ufa: Monografia, 2007.
16. Panin, V.E., Elsukova, T.F., and Popkova, Yu.F., Channeled Local Structural Transformations in Polycrystal Surface Layers in Alternate Cyclic Bending, *Phys. Mesomech.*, 2011, vol. 14, no. 1–2, pp. 1–9.